International Journal of Power Electronics and Drive System (IJPEDS)
Vol. 17, No. 2, June 2026, pp. 1130~1141
ISSN: 2088-8694, DOI: 10.11591/ijpeds.v17.i2.pp1130-1141

Design and performance evaluation of a soft-switched partial-power LLC converter for PV grid integration

Sebin Davis Kurichiparambil, Varghese Jegathesan
Department of Electrical and Electronics Engineering, Karunya Institute of Technology and Sciences, Coimbatore, India

Article Info

Article history:

Received Jun 10, 2025
Revised Apr 2, 2026
Accepted Apr 23, 2026

Keywords:

Grid integration
Grid-tied inverter
LLC resonant converter
Photovoltaic
Three-phase inverter
Two-stage PV inverter

ABSTRACT

This paper presents a soft-switched partial-power LLC converter integrated within a two-stage photovoltaic (PV) and grid-connected system. The proposed architecture combines the advantages of resonant operation and partial power processing to enhance conversion efficiency and reduce switching losses. Maximum power point tracking (MPPT) is achieved through frequency modulation of the LLC converter, while grid synchronization is maintained using a three-phase voltage-oriented control (VOC) inverter. Simulation results in MATLAB/Simulink demonstrate stable zero voltage switching (ZVS) and zero current switching (ZCS) across a wide irradiance range (400-1000 W/m²), enabling the system to achieve peak efficiencies above 98%, which is superior to typical transformerless and interleaved converter topologies reported in recent literature. The proposed soft-switched PPC–LLC architecture offers an efficient and scalable solution for next-generation PV grid interfaces by combining reduced processed power, robust resonant operation, and high-quality grid integration.

Corresponding Author:

Sebin Davis Kurichiparambil
Department of Electrical and Electronics Engineering, Karunya Institute of Technology and Sciences
Karunya Nagar, Coimbatore, Tamil Nadu 641114, India
Email: sebindavisk@gmail.com

1. INTRODUCTION

Achieving high-efficiency grid integration in photovoltaic (PV) systems remains a major challenge due to conversion losses and limited dynamic control in existing power electronic converters. Grid-connected PV systems are usually classified as either single-stage or two-stage based on their processing stages, as shown in Figures 1(a) and 1(b), respectively [1], [2]. The single-stage topology uses one inverter for both maximum power point tracking (MPPT) and grid integration, seen as the most reliable and cost-effective structure [3]. However, operational limitations arise due to the minimum DC-link voltage required for grid-connected inverter operation and the rated voltage of switches, imposing constraints on MPPT operations [4]. Two-stage systems overcome this limitation through an additional DC–DC converter, which improves MPPT range but increases conduction and switching losses [5], [6].

An additional stage in the two-stage configuration contributing to losses, designing this additional conversion stage with higher efficiency beyond 98%, and leveraging an enhanced energy output from MPPT, minimizes the impact of the power converter on overall efficiency [7]. Recent works on transformerless and multilevel inverter systems have improved power quality but have not adequately addressed conversion losses in the DC-DC stage. Therefore, there exists a research gap in developing a soft-switched, high-efficiency DC-DC converter architecture capable of processing only a fraction of the total PV power while maintaining effective MPPT and grid integration [8]. To address this, the present work proposes a half-bridge

series LLC resonant converter integrated by a partial power processing (PPC) structure in the DC-DC stage. The design achieves soft switching zero voltage switching/zero current switching (ZVS/ZCS) and frequency-controlled MPPT while ensuring efficient grid synchronization through a voltage-oriented control (VOC) inverter. However, existing PPC-LLC-based PV converter architectures do not provide an improved solution that achieves soft-switching across wide irradiance variations and ensures stable grid integration through an inverter control framework.

Inverter current control is crucial as it should be conditioned according to grid conditions, including phase sequence, phase angle, and total harmonic distortion, as per grid standards [9], [10]. In a grid-connected PV system, the voltage source inverter (VSI) maintains the DC-link voltage at its reference value by regulating active and reactive power [11]. Using a synchronous d–q reference frame with Park transformation, the VOC method synchronizes the inverter output with the grid [12]. Aligning the grid voltage vector along the d-axis allows independent control of active and reactive currents, ensuring unity power factor and stable operation [13], [14].

The structure of the paper is as follows: i) The motivation and backdrop are presented in Section 1; ii) Section 2 explains the design of the partial power processing utilizing a half-bridge LLC resonant converter and the MPPT algorithm; iii) Section 3 details the control strategy for the voltage-oriented control inverter connected to the grid; iv) Section 4 presents simulation results under varying irradiance conditions, verifying soft-switching, MPPT effectiveness, and grid synchronization; and v) Section 5 concludes with key findings and performance highlights.

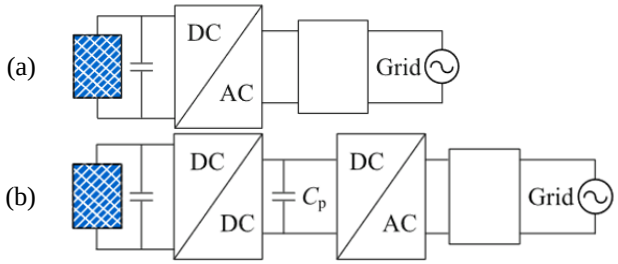

Figure 1. PV inverter configurations: (a) single-stage and (b) two-stage

2. PARTIAL POWER CONVERTER AND MPPT ALGORITHM

In a full power converter (FPC) system, both the DC-DC and DC-AC converter stages handle the whole power PV system that delivers electricity to the grid [15]. However, the additional stage introduces extra conduction, switching, and magnetic losses, which reduce the efficiency of the converter along with the power handling capacity of each converter. Partial-power processing (PPP) operates on the principle that only a fraction of the total power is managed by a DC-DC converter, whereas the majority of energy transfers directly from the source to the output without undergoing processing [16]. In a series-connected partial-power converter (S-PPC), the input source and the DC-DC converter's output are connected in series [17], [18].

For the S-PPC converter, an isolated DC-DC converter serves as a fundamental circuit component and is customized for its specific operational requirements. Resonant converters based on high-frequency transformers deliver enhanced efficiency across a broad spectrum of loads and offer galvanic isolation, which makes it highly suitable for the PPC topologies [19]. The output voltage of the resonant converter is regulated by adjusting its switching frequency. Soft-switched resonant converters typically offer improved efficiency compared to hard-switched DC/DC topologies, and the availability of galvanic isolation enables the half-bridge series LLC to be particularly well-suited for S-PPC topologies. ZVS and ZCS techniques reduce the switching losses of LLC resonant converters, thereby enhancing DC/DC converter stage efficiency [20].

2.1. Proposed DC/DC converter

The proposed structure of two-stage PV systems mainly consists of a half-bridge series LLC resonant converter along with PPC topology in the DC/DC stage. The input is connected in series with the secondary side of the HB series LLC resonant converter for the development of PPC. The LLC resonant converter has a resonant tank consisting of C_r and L_r, the primary resonant capacitor and primary resonant inductor, respectively, and L_m, the magnetizing inductor. In an LLC resonant converter, the resonant frequency f_r of the resonant tank is determined by (1).

$$f_r = \frac{1}{2\pi\sqrt{L_r C_r}} \quad (1)$$

Voltage gain (G_{LLC}) of the LLC resonant tank depends on the quality factor (Q_e), ratio of entire primary inductance to resonant inductance (m), and ratio of switching frequency to normalized resonant frequency (f_n).

$$G_{LLC} = \frac{f_n^2(m-1)}{\sqrt{(mf_n^2-1)^2+f_n^2.(f_n^2-1)^2.(m-1)^2.Q^2}} \quad (2)$$

$$Qe = \frac{\sqrt{L_r/C_r}}{R_e} \quad (3)$$

$$m = \frac{L_m+L_r}{L_r} \quad (4)$$

$$f_n = \frac{f_s}{f_r} \quad (5)$$

Kirchhoff's laws are applied to the S-PPC configuration, as shown in Figure 2, to determine the voltage gain of the proposed converter. The portion of active power handled by the DC-DC converter compared with the source input power to the DC-DC stage is known as the partial power ratio (K_{pr}) as (6).

$$K_{pr} = \frac{V_{pv}I_{conv}}{V_{pv}I_{in}} \quad (6)$$

Where V_{pv}: PV array output voltage, I_{conv}: converter output current, I_{in}: PV array output current, and n = transformer ratio. The HB-LLC series resonant converter voltage gain G_{conv} can be expressed as (7).

$$G_{Conv} = \frac{G_{LLC}}{2n} \quad (7)$$

The proposed converter voltage gain can be written as (8).

$$\frac{V_{dc}-V_{pv}}{V_{pv}} = \frac{G_{LLC}}{2n} \quad (8)$$

The voltage gain of the total DC-DC converter stage, the global gain, G_v can be expressed as (9).

$$G_v = 1 + \frac{G_{LLC}}{2n} \quad (9)$$

The behaviour of the voltage gain function for changing values of Q_e is shown in Figure 3. The LLC resonant converter operates within a specific frequency range that is primarily determined by the resonant frequency (f_0) and the peak gain frequency (f_p). The converter typically operates around its resonant frequency to minimize switching losses and achieve zero voltage switching (ZVS) over a wide range of loads and input conditions. The peak gain occurs between f_p and f_0, and this frequency range can vary based on load conditions (Q_e) and the ratio between the magnetizing inductance (L_m) and the primary leakage inductance L_r. Since Kpr is directly proportional to the voltage gain, operation close to Gv=1 helps to keep Kpr values low to improve overall efficiency and reduce the power-handling requirement of the PPC stage. Lower Kpr values allow the dc–dc stage to be designed with reduced converter size, while also ensuring minimal resonant-tank current, device stress, and thermal loading.

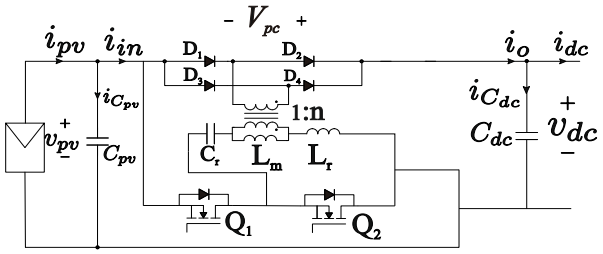

Figure 2. Proposed partial power converter

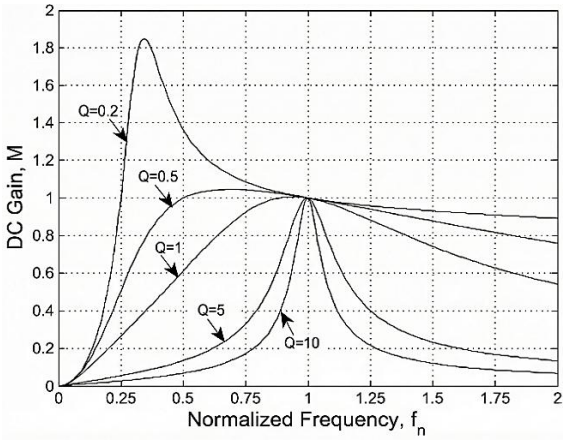

Figure 3. Behavior of the voltage gain function

2.2. MPPT algorithm

Depending on the switching frequency, the LLC resonant tank runs in either boost or buck mode. If the converter switching frequency is higher than the resonant frequency, the converter functions in buck mode [21]. Conversely, when the switching frequency is lower than the resonant frequency, the converter functions in boost mode. MPPT tracking is accomplished by adjusting the switching frequency to achieve the maximum power from the DC-DC stage. By adjusting the switching frequency, the MPPT controller raises or lowers the converter gain in response to variations in solar irradiation in order to achieve the new maximum power point. Integration of frequency-modulated MPPT control within the PPC–LLC converter enables simultaneous soft-switching and partial power processing, creating a unique system configuration.

The flowchart of the perturb and observe (P&O) method, illustrated in Figure 4, begins by measuring the PV voltage, $V_{pv}(n)$, and the PV current, Ipv(n), in the nth cycle to determine the PV power, $P_{pv}(n)$. Subsequently, $P_{pv}(n)$ and $V_{pv}(n)$ are compared with the PV power, $P_{pv}(n-1)$, and the PV voltage, $V_{pv}(n-1)$, from the previous cycle. Therefore, the frequency perturbation Δfs is adjusted to either increase or decrease. Applying a small perturbation improves tracking accuracy but reduces tracking speed. On the other hand, using a large perturbation enhances tracking speed but decreases tracking accuracy. Therefore, optimal perturbation is applied based on the total PV power.

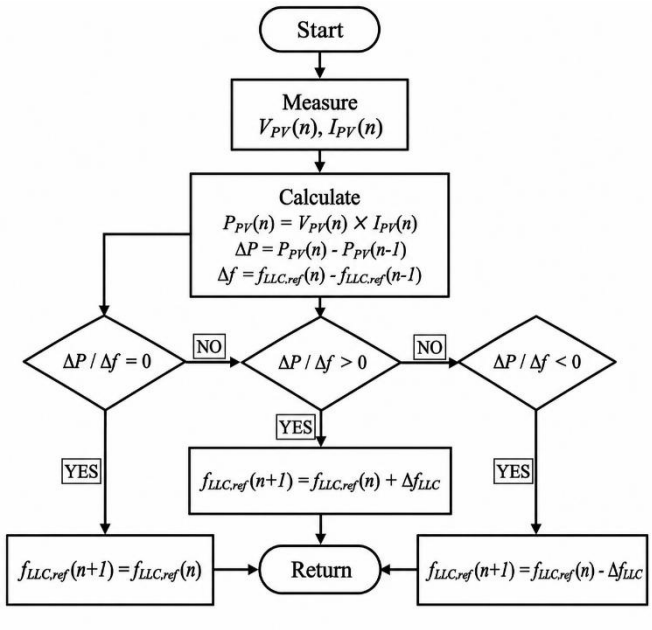

Figure 4. Proposed MPPT algorithm

3. THREE-PHASE INVERTER CONTROL STRATEGY

The second stage of the proposed two-stage PV system uses a self-commutated inverter VSI in the proposed design for power conversion and optimizing control. It is managed using the VOC method, which models the VSI as a controlled AC voltage source. This control system utilizes a double-loop control mode, featuring an inner current loop for regulating both active current (Id) and reactive current (Iq) and an outer voltage loop. The control strategy, implemented in the dq synchronous reference frame, simplifies control by converting grid measurements into direct current (DC) values. To synchronize injected currents with grid voltages and enable the abc-dq transformation, a phase-locked loop (PLL) extracts the crucial phase angle of the grid voltage.

This double-loop control system with proportional-integral (PI) controllers regulates both grid current and DC-link voltage (Vdc) [22]. The outer voltage loop stabilizes Vdc, and its output becomes the reference value for active current (Id). To further simplify control of active and reactive currents (Id and Iq), a feed-forward decoupling strategy is implemented. Notably, setting the reactive current reference (Iq) to zero ensures the grid inverter operates at unity power factor (PF).

3.1. Modelling of the three-phase VSI

Considering access to the power grid through an RL filter (R + jωL) as shown in Figure 5, the following equations describe the grid inverter voltages as (10).

$$\begin{aligned} V_{ia} &= L\frac{di_a}{dt} + Ri_a + V_{ga} \\ V_{ib} &= L\frac{di_b}{dt} + Ri_b + V_{gb} \\ V_{ic} &= L\frac{di_c}{dt} + Ri_c + V_{gc} \end{aligned} \quad (10)$$

Where "V_{ga}, V_{gb}, V_{gc}", "i_a, i_b, i_c," and "V_{ia}, V_{ib}, V_{ic}" are grid voltage, inverter current, and inverter voltage, respectively. By applying the d-q transformation, the mathematical model of the grid inverter in the d-q synchronous reference frame can be obtained as (11).

$$\begin{aligned} V_{id} &= L\frac{di_d}{dt} + Ri_d - \omega Li_q + V_{gd} \\ V_{iq} &= L\frac{di_q}{dt} + Ri_q + \omega Li_d + V_{gq} \end{aligned} \quad (11)$$

For power calculations, the grid-side active and reactive power equations expressed in space vector form are given by (12).

$$\begin{aligned} P &= \frac{3}{2}\left(V_d I_d + V_q I_q\right) \\ Q &= \frac{3}{2}\left(V_q I_d - V_d I_q\right) \end{aligned} \quad (12)$$

The direct components of the grid voltage and current are represented by V_d and I_d, respectively, while V_q and I_q denote the quadrature components of the grid voltage and current. As the system has to operate at unity power factor in normal conditions, power losses can be neglected. Then, V_q is zero for a balanced system. Thus, the equations become (13).

$$\begin{aligned} P &= \frac{3}{2}(V_d I_d) \\ Q &= -\frac{3}{2}\left(V_d I_q\right) \end{aligned} \quad (13)$$

3.2. Grid inverter control strategy

Maintaining a constant DC-link voltage ensures optimal power transfer from the DC side to the AC side, confirming efficient operation [23]. This approach is widely used in PV systems with a continuous power supply from PV arrays, guaranteeing maximum power delivery to the load. In grid-tied applications, the DC-link voltage must be higher than the peak grid voltage to facilitate proper power injection [24]. According to the instantaneous power theory, a lossless power converter must balance input and output power, ensuring efficient energy conversion.

Input DC power = Output AC power

$$V_{dc}C_{dc}\frac{dV_{dc}}{dt} = \frac{3}{2}\left(I_d V_d + I_q V_q\right) \quad (14)$$

By aligning the dq reference frame's rotational speed with the grid frequency, the transformed variables remain steady in a stable state, streamlining controller implementation. This synchronization is accomplished through a PLL, which takes an alternating grid voltage as input and produces the phase angle necessary for abc-to-dq conversion. Assuming that the PLL accurately tracks the output voltage vector, aligning the d-axis of the synchronous dq reference frame such that Vq=0, the transfer functions can be derived [25]. These transfer functions represent the relationship between the DC-link voltage output, reactive power, and the d-axis current. They can be expressed as (15):

$$\frac{V_{dc}(s)}{I_d(s)} = \frac{3}{2}\frac{V_d(s)}{sV_{dc}C_{dc}} \tag{15}$$

There exists an interaction between the d-axis and q-axis components, which can impact the controller's dynamic response. To enhance performance, it is crucial to eliminate this cross-coupling effect. A feedforward compensation-based decoupling strategy can be implemented to achieve independent control of both axes.

The cross-coupling can be decoupled by (4). Hence, the d-axis currents id and q-axis currents iq can be controlled independently by reference current id* and iq*, respectively. As a result, PI controllers are employed to ensure a rapid dynamic response while maintaining zero steady-state error. As a result, PI controllers are implemented to provide a fast dynamic response and eliminate steady-state errors. The transfer function of the grid-connected VSI can be expressed as (16).

$$G_p(S) = \frac{1}{(T_s s+1)(Ls+R} \tag{16}$$

For precise and rapid tracking of the current signal, the current loop must exhibit strong performance. For R = 0.1 Ω, *L* = 3 mH, *T*s = 0.167 ms, and design is based on the system type 1 for a damping ratio of 0.707 to ensure optimal stability and response, the transfer function of the PI controller is given by (17).

$$G_{pi}(z) = \frac{9z-8.95}{z-1} \tag{17}$$

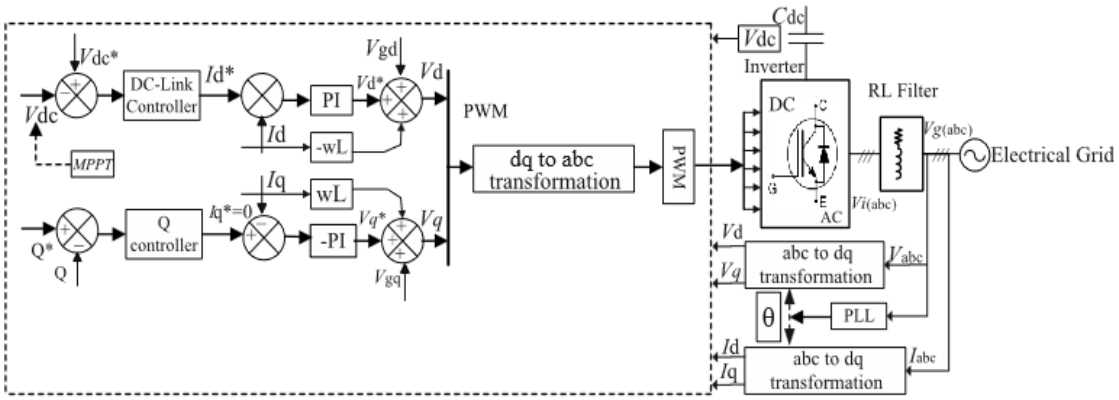

Figure 5. PV inverter control algorithm

4. SIMULATION RESULTS AND DISCUSSION

The proposed PV grid-connected system was simulated in MATLAB/Simulink to verify the performance of the converter architecture, with special focus on the DC-DC stage. The DC-DC converter employs a half-bridge series LLC resonant topology integrated with PPC, designed to operate under soft-switching conditions. The schematic diagram of the model used for the simulation study is shown in Figure 6. This stage plays a crucial role in both efficient energy conversion and successful MPPT implementation, making it central to the overall system performance. The P&O method is implemented in real-time to adjust the operating frequency such that the PV panel consistently operates at or near its maximum power point, despite variations in irradiance.

A two-stage PV inverter with a three-phase VSI grid-connected inverter in the DC-AC stage, and a half-bridge series LLC resonant converter with PPC topology in the first stage is modelled in this section. A simulation study is conducted in the model based on the theoretical basis of analysis done in the previous

chapters. In order to accomplish the proposed two-stage grid-connected inverter with a power capacity of 100 kW, the PV system array consists of 18 parallel strings and 18 PV modules connected in series. The main parameters of the selected PV panel are shown in Table 1. Waaree Energies WSM-315 model PV module was selected from MATLAB/Simulink to realize the 100 kW PV array system for the simulation environment.

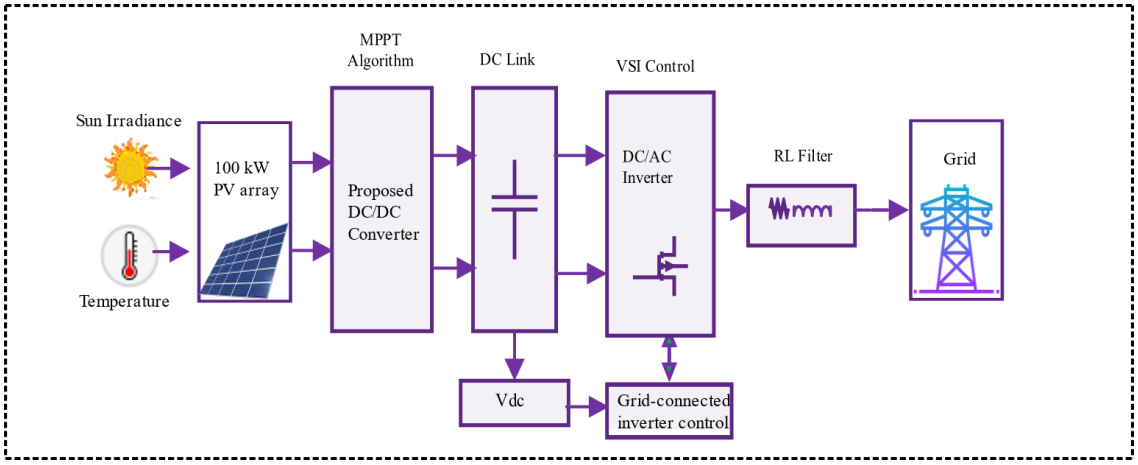

Figure 6. Schematic-diagram of grid connected voltage source inverter

Table 1. PV module main parameters

Parameters of the PV module	Value
Nominal maximum power (Pmax)	315 W
Optimum operating voltage (Vmp)	35 V
Optimum operating current (Imp)	9 A
Open circuit voltage (Voe)	43 V
Short circuit current (lsc)	9.77 A
No of cell	72 Nos

A 100 kW half-bridge LLC resonant converter is implemented as part of a series partial power converter (SPPC) topology, with a transformer of a 1:1 turns ratio and operating over a switching frequency range of 72 kHz to 120 kHz. The resonant frequency is set at 120 kHz to enable soft switching, ensuring ZVS for the primary switches and ZCS for the secondary rectifier. The resonant tank consists of a resonant capacitor Cr of 380 nF, a resonant inductor Lr of approximately 4.63 µH, and a magnetizing inductance Lm of 23.15 µH, maintaining an Lm/Lr ratio of 5. The converter operates with a variable switching frequency to implement MPPT, while the output DC bus voltage is regulated at 600 V through the voltage control loop of the grid-tied inverter. The grid-tied inverter design parameters listed in Table 2 are applied to the DC/AC stage of the simulation. The MATLAB blocks used in simulation studies of the above topology and control are shown in Figure 7.

The simulation was conducted under different irradiance conditions: 400, 600, 800, and 1000 W/m². In all cases, the LLC converter was able to dynamically adjust its frequency to ensure optimal power extraction. The MPPT also shows fast convergence, settling to the new operating point within approximately 8–12 ms during irradiance changes. The converter maintains a stable output at 600 V DC, which is fed into the DC-link capacitor and subsequently into the three-phase inverter. The applied irradiance, along with the output active and reactive power fed to the grid, is shown in Figure 8. The effective operation of the voltage controller, which helps to maintain the DC bus voltage at 600 V and thus ensures the maximum power available in the PV array, is also visible in Figure 7. A key advantage of the LLC topology in this system is its ability to operate under soft switching across a wide input power range. The resonant inductor current (Ir) and magnetizing current (Im) waveforms were shown in Figure 9 at each irradiance level. The results confirm that ZVS for the primary switches and ZCS for the secondary-side rectifiers were consistently achieved. Soft switching was maintained even under low irradiance (400 W/m²), demonstrating the robustness of the design. The system was tested for temperature variations (25–60 °C) and ±20% load changes, maintaining ZVS/ZCS operation and DC-link voltage stability within ±2% of the reference.

Table 2. Parameters of the grid-connected three-phase inverter

Parameter	Value
Grid line voltage	400 V
Grid frequency	50 Hz
DC-link-voltage	600 V
DC bus capacitance	0.22F
Filter inductor	0.1 mH
Filter resistance	0.2 mΩ
Switching frequency	2 kHz
PI parameter of the current loop	Kp = 0.3, Ki = 20
PI parameter of the voltage loop	Kp = 2, Ki = 400

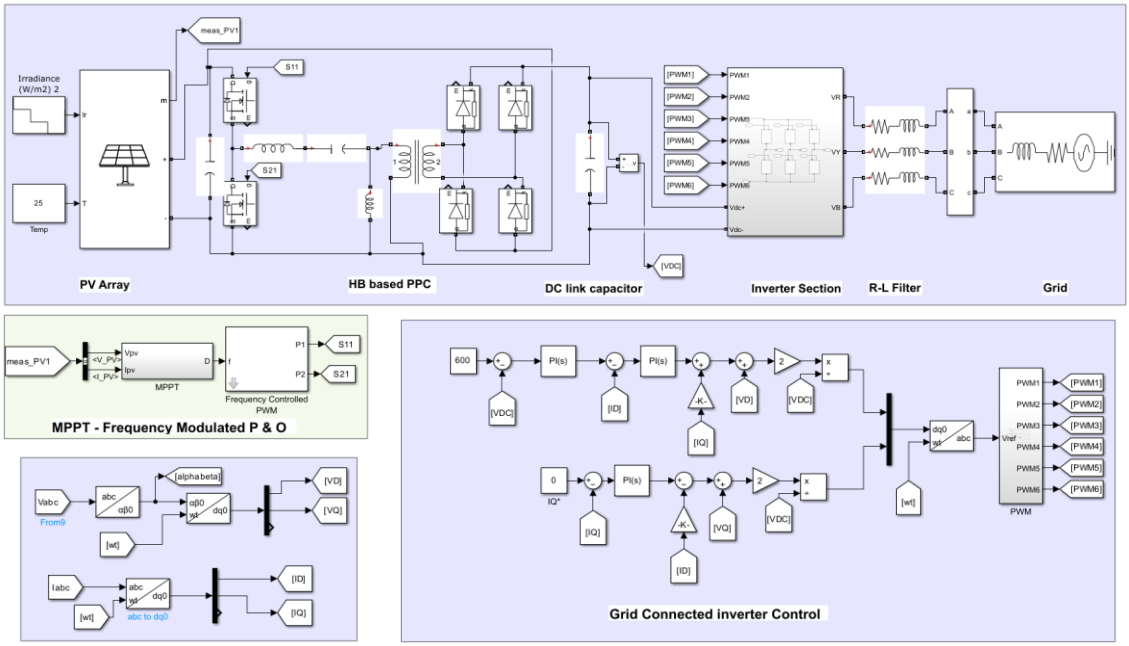

Figure 7. PV grid-connected system with partial-power LLC converter simulated using MATLAB Simulink

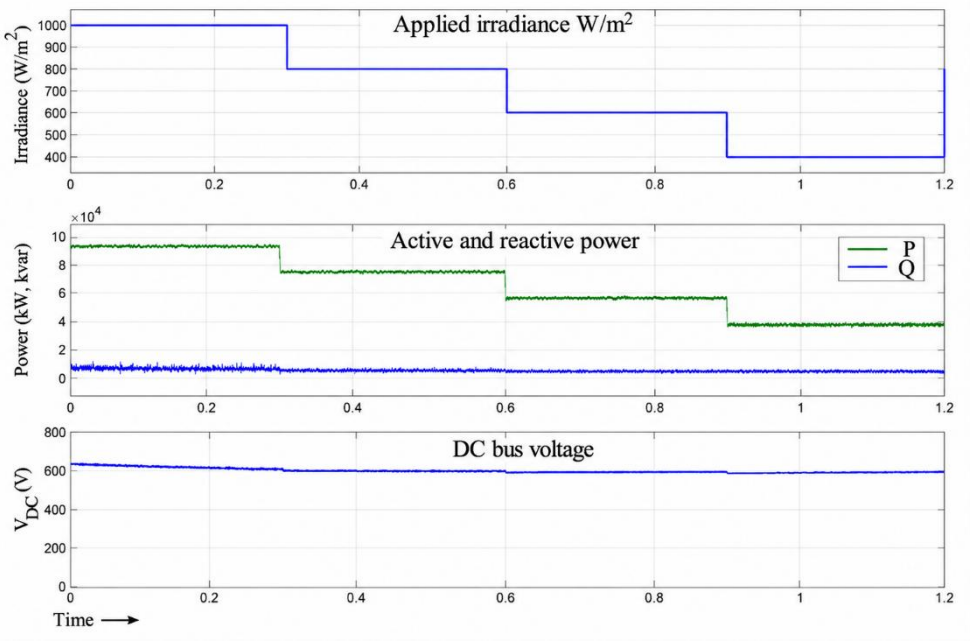

Figure 8. Simulation response of power and DC bus voltage for varying irradiance

At 1000 W/m², the converter achieved a peak efficiency of 98.32%. Notably, even at reduced irradiance levels of 800, 600, and 400 W/m², the efficiencies remained high: 98.29%, 98.34%, and 97.86%, respectively. The DC–DC stage using the half-bridge LLC resonant converter with PPC achieved a higher efficiency of 98.1–99.3%, while the DC–AC stage employing the three-phase VSI maintained an efficiency range of 98.0–98.9%. In the case of 1000 W/m² and 25 °C, the PV array supplies about 101 kW DC, from which the inverter delivers 99.3 kW AC to the grid. Only 24.6 kW is processed by the PPC–LLC stage (25.9% of total power), yet the converter maintains soft switching and achieves up to 99.3% efficiency, due to lower switching losses. The PPC architecture contributes significantly to this result by ensuring that only a portion of the total power flows through the high-frequency switching stage, thereby reducing conduction losses and improving system-level efficiency. The three-phase voltage source inverter (VSI) forms the second stage of the system and is used for grid integration. It operates under a VOC scheme that ensures synchronization with the grid and maintains a unity power factor.

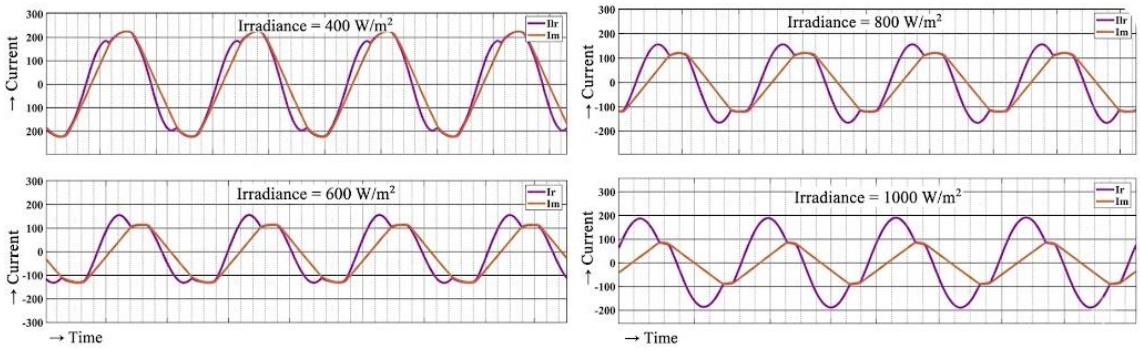

Figure 9. Key operation waveform of the LLC at different irradiance levels

Simulated waveforms at the point of common coupling (PCC) show well-shaped sinusoidal voltages and currents, with minimal distortion, as shown in Figure 10. The grid receives active power efficiently, with reactive power near zero under all irradiance levels. Power waveforms further validate that the system responds effectively to changes in irradiance. The MPPT loop quickly adapts to variations, ensuring minimal mismatch between PV generation and grid power output. The combined performance of the LLC-PPC converter and the inverter demonstrates that the proposed topology can maintain high efficiency, reliable grid interface, and excellent power quality. Figure 11 presents the harmonic spectrum of the inverter output current, showing a THD of 2.45%, which is not only well within the IEEE 1547 grid interconnection limit.

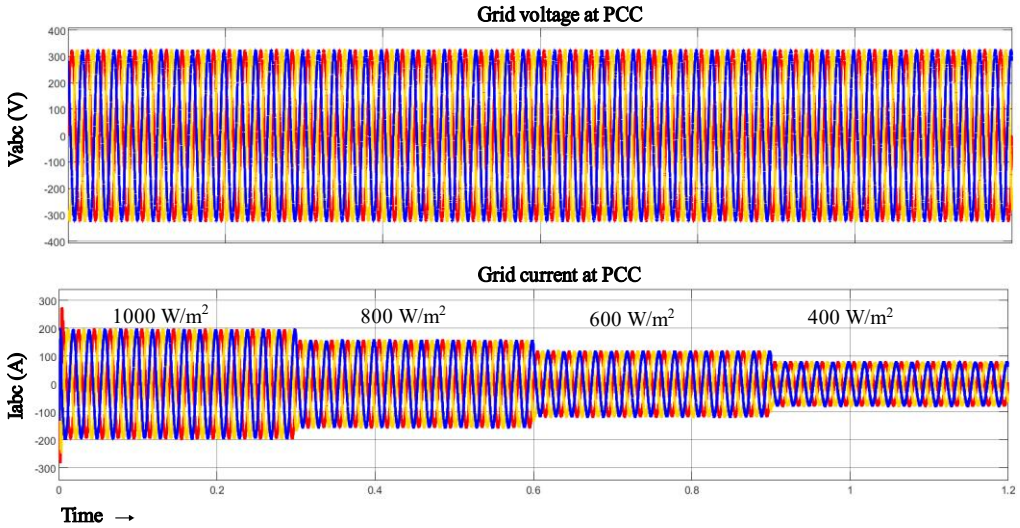

Figure 10. Injected grid voltages and currents under varying irradiance

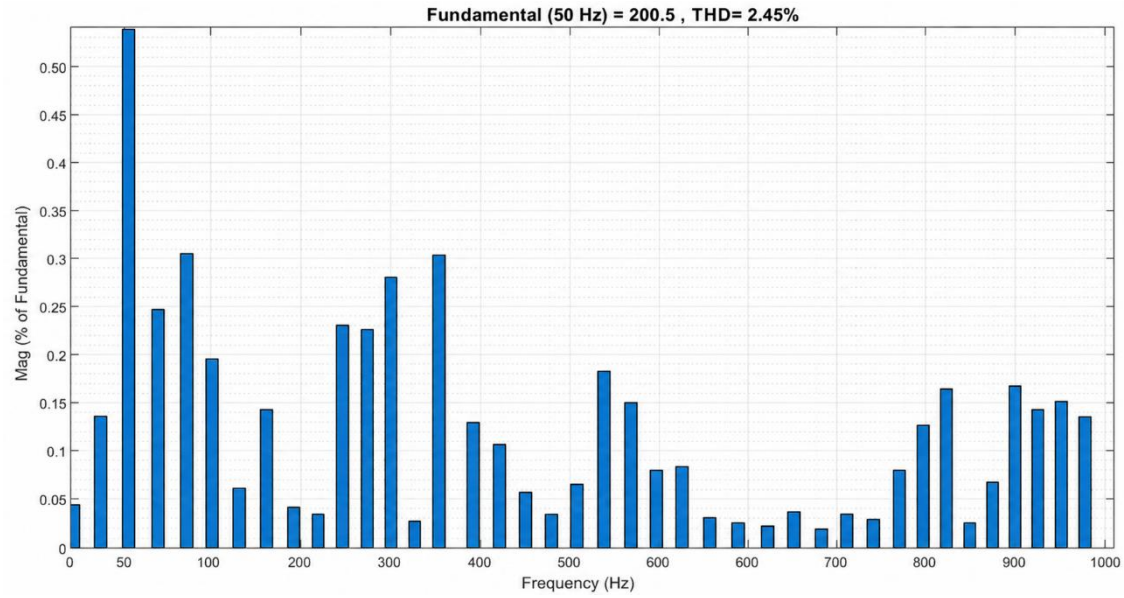

Figure 11. Harmonic analysis of inverter output current using FFT

The proposed system has been designed with a practically implementable switching frequency range, and the control algorithm is suitable for real-time execution on digital control platforms such as DSP or FPGA. Table 3 [24]-[26] compares the proposed PPC–LLC converter with advanced MPPT and inverter control methods, showing its clear advantages in efficiency and overall performance. The proposed PPC–LLC converter achieved a peak efficiency of 98.32% at 1000 W/m², which is higher than values reported for transformerless PV inverters (97–98%) [24]) and comparable to high-frequency GaN-based resonant converters (98–99% [27]) while using only silicon devices. Interleaved DC–DC converter–based systems typically report 97–98% efficiency [28], indicating that the PPC–LLC architecture provides a measurable improvement of 1–1.3% over conventional silicon-based topologies. The PPC–LLC architecture is scalable to MW-level PV systems through integration of converter units and parallel operation of inverter stages, enabling high efficiency and soft-switching performance at higher power levels.

Table 3. Comparative evaluation of PPC–LLC converter

Model	MPPT response time	Efficiency (%)	THD (%)	Control complexity	System cost
VOC + ANN MPPT [24]	5–12 ms	97–98%	2–3%	High	Medium–High
Predictive control (MPC) + Inc-Cond [25]	10–20 ms	94–96%	1.5–3%	Very high	High
Predictive control + Fuzzy MPPT [26]	10–15 ms	95–97%	1–2.5%	Very high	High
Proposed method PPC–LLC + VOC	8–12 ms	98.3%	2- 3%	Medium	Low–Medium

5. CONCLUSION

A high-efficiency two-stage PV grid-connected system is presented, integrating a Half-Bridge Series LLC resonant converter with PPC to enable soft switching and frequency-based MPPT, while a VOC-controlled voltage source inverter ensures stable grid integration. The converter consistently achieves ZVS/ZCS across a wide irradiance range, reducing switching losses and improving overall efficiency, and the combined MPPT–VOC framework maintains rapid power tracking, DC-link stability, and unity power factor during grid operation. The novelty of this work lies in unifying partial power processing, resonant soft switching, and a fully modeled grid-integration strategy within a single system-level architecture. However, the study is limited to simulation, and hardware validation, as well as detailed thermal and stress analysis, remain for future investigation. Future research will focus on experimental implementation, adaptive MPPT strategies, and expanded grid-support functions such as LVRT capability. Overall, the PPC–LLC architecture demonstrates strong potential as a scalable and high-efficiency solution for next-generation PV grid interfaces.

FUNDING INFORMATION

Authors state no funding involved.

AUTHOR CONTRIBUTIONS STATEMENT

This journal uses the Contributor Roles Taxonomy (CRediT) to recognize individual author contributions, reduce authorship disputes, and facilitate collaboration.

Name of Author	C	M	So	Va	Fo	I	R	D	O	E	Vi	Su	P	Fu
Sebin Davis Kurichiparambil	✓	✓	✓	✓	✓	✓	✓	✓	✓	✓	✓		✓	
Varghese Jegathesan	✓	✓		✓	✓	✓				✓	✓	✓		

C : **C**onceptualization
M : **M**ethodology
So : **So**ftware
Va : **Va**lidation
Fo : **Fo**rmal analysis
I : **I**nvestigation
R : **R**esources
D : **D**ata Curation
O : Writing - **O**riginal Draft
E : Writing - Review & **E**diting
Vi : **Vi**sualization
Su : **Su**pervision
P : **P**roject administration
Fu : **Fu**nding acquisition

CONFLICT OF INTEREST STATEMENT

The authors declare no conflict of interest.

DATA AVAILABILITY

Derived data supporting the findings of this study are available from the corresponding author, [SDK], on request.

REFERENCES

[1] Z. Yao and Z. Wang, "Single-stage doubly grounded transformerless PV grid-connected inverter with boost function," *IEEE Transactions on Power Electronics*, vol. 37, no. 2, pp. 2237–2249, 2022, doi: 10.1109/TPEL.2021.3105059.

[2] H. Hasabelrasul, Z. Cai, L. Sun, X. Suo, and I. Matraji, "Two-stage converter standalone PV-battery system based on VSG control," *IEEE Access*, vol. 10, pp. 39825–39832, 2022, doi: 10.1109/ACCESS.2022.3165664.

[3] S. Ponrekha A., M. S. P. Subathra, C. Bharatiraja, N. Manoj Kumar, and H. Haes Alhelou, "A topology review and comparative analysis on transformerless grid-connected photovoltaic inverters and leakage current reduction techniques," *IET Renewable Power Generation*, vol. 19, no. 1, Jan. 2025, doi: 10.1049/rpg2.12655.

[4] S. Nyamathulla and D. Chittathuru, "A review of multilevel inverter topologies for grid-connected sustainable solar photovoltaic systems," *Sustainability*, vol. 15, no. 18, p. 13376, Sep. 2023, doi: 10.3390/su151813376.

[5] P. Ezhilvannan, S. Krishnan, B. H. Kumar, K. Janardhan, and S. Ramachandran, "Analysis of the effectiveness of a two-stage three-phase grid-connected inverter for photovoltaic applications," *Journal of Solar Energy Research*, vol. 8, no. 2, pp. 1471–1483, 2023, doi: 10.22059/jser.2023.357025.1285.

[6] N. Tak and S. K. Chattopadhyay, "Two-stage three-phase transformerless hybrid multilevel inverter for solar PV application," *IEEE Transactions on Industrial Electronics*, vol. 71, no. 6, pp. 5386–5398, Jun. 2024, doi: 10.1109/TIE.2023.3299027.

[7] F. Marignetti, R. L. Di Stefano, G. Rubino, and R. Giacomobono, "Current source inverter (CSI) power converters in photovoltaic systems: a comprehensive review of performance, control, and integration," *Energies*, vol. 16, no. 21, p. 7319, Oct. 2023, doi: 10.3390/en16217319.

[8] M. Daryaei, M. Esteki, and S. A. Khajehoddin, "High efficiency and full MPPT range partial power processing PV module-integrated converter," *IEEE Transactions on Power Electronics*, vol. 38, no. 5, pp. 6627–6641, May 2023, doi: 10.1109/TPEL.2023.3243174.

[9] P. M. Robina, K. Rouzbehi, F. Gordillo, and J. Pou, "Grid-following voltage source converters: basic schemes and current control techniques to operate with unbalanced voltage conditions," *IEEE Open Journal of the Industrial Electronics Society*, vol. 2, pp. 528–544, 2021, doi: 10.1109/OJIES.2021.3121764.

[10] S. Haq *et al.*, "An advanced PWM technique for MMC inverter based grid-connected photovoltaic systems," *IEEE Transactions on Applied Superconductivity*, vol. 31, no. 8, pp. 1–5, Nov. 2021, doi: 10.1109/TASC.2021.3094439.

[11] F. J. Zimann, A. L. Batschauer, M. Mezaroba, and F. A. S. Neves, "Energy storage system control algorithm for voltage regulation with active and reactive power injection in low-voltage distribution network," *Electric Power Systems Research*, vol. 174, p. 105825, Sep. 2019, doi: 10.1016/j.epsr.2019.04.003.

[12] I. Jamal, M. F. Elmorshedy, S. M. Dabour, E. M. Rashad, W. Xu, and D. J. Almakhles, "A comprehensive review of grid-connected PV systems based on impedance source inverter," *IEEE Access*, vol. 10, pp. 89101–89123, 2022, doi: 10.1109/ACCESS.2022.3200681.

[13] R. Bisht, R. Bhattarai, S. Subramaniam, and S. Kamalasadan, "A novel synchronously rotating reference frame based adaptive control architecture for enhanced grid support functions of single-phase inverters," *IEEE Transactions on Industry Applications*, vol. 56, no. 4, pp. 4288–4298, Jul. 2020, doi: 10.1109/TIA.2020.2994879.

[14] A. Majumder and S. Chowdhuri, "Development of hybrid SOGI-resonant controller in DQ reference frame for decoupled PQ control of a VSI under nonlinear loading," *Electrical Engineering*, vol. 107, pp. 3359–3373, Sep. 2024, doi: 10.1007/s00202-024-02688-y.

[15] N. G. F. dos Santos, J. R. R. Zientarski, and M. L. da S. Martins, "A review of series-connected partial power converters for DC–DC applications," *IEEE Journal of Emerging and Selected Topics in Power Electronics*, vol. 10, no. 6, pp. 7825–7838, Dec. 2022, doi: 10.1109/JESTPE.2021.3082869.
[16] P. Granello, T. B. Soeiro, N. H. van der Blij, and P. Bauer, "Revisiting the partial power processing concept: case study of a 5-kW 99.11% efficient flyback converter-based battery charger," *IEEE Transactions on Transportation Electrification*, vol. 8, no. 3, pp. 3934–3945, Sep. 2022, doi: 10.1109/TTE.2022.3170286.
[17] Y. D. Kwon, F. D. Freijedo, T. Wijekoon, and M. Liserre, "Series resonant converter-based full-bridge DC–dc partial power converter for solar PV," *IEEE Journal of Emerging and Selected Topics in Power Electronics*, vol. 12, no. 2, pp. 1719–1729, Apr. 2024, doi: 10.1109/JESTPE.2024.3355511.
[18] N. Yadav *et al.*, "Performance evaluation of step-up/down partial power converters based on current-fed DC-DC topologies," *IEEE Transactions on Industry Applications*, vol. 60, no. 5, pp. 7111–7124, Sep. 2024, doi: 10.1109/TIA.2024.3413050.
[19] D. Pesantez, H. Renaudineau, S. Rivera, A. Peralta, A. Marquez Alcaide, and S. Kouro, "Transformerless partial power converter topology for electric vehicle fast charge," *IET Power Electronics*, vol. 17, no. 8, pp. 970–982, Jun. 2024, doi: 10.1049/pel2.12613.
[20] J. Shahsevani and R. Beiranvand, "Application-oriented review of the LLC-based resonant converters," *IEEE Access*, vol. 12, pp. 52687–52726, 2024, doi: 10.1109/ACCESS.2024.3386430.
[21] G. Li, J. Xia, K. Wang, Y. Deng, X. He, and Y. Wang, "Hybrid modulation of parallel-series LLC resonant converter and phase shift full-bridge converter for a dual-output DC–DC converter," *IEEE Journal of Emerging and Selected Topics in Power Electronics*, vol. 7, no. 2, pp. 833–842, Jun. 2019, doi: 10.1109/JESTPE.2019.2900700.
[22] X. Zhou, Q. Liu, Y. Ma, and B. Xie, "DC-link voltage research of photovoltaic grid-connected inverter using improved active disturbance rejection control," *IEEE Access*, vol. 9, pp. 9884–9894, 2021, doi: 10.1109/ACCESS.2021.3050191.
[23] K. Ben Hamad, D. N. Luta, and A. K. Raji, "A grid-tied fuel cell multilevel inverter with low harmonic distortions," Energies, vol. 14, no. 3, p. 688, Jan. 2021, doi: 10.3390/en14030688.
[24] N. F. Ibrahim *et al.*, "Operation of grid-connected PV system with ANN-based MPPT and an optimized LCL filter using GRG algorithm for enhanced power quality," *IEEE Access*, vol. 11, pp. 106859–106876, 2023, doi: 10.1109/ACCESS.2023.3317980.
[25] N. Kacimi, A. Idir, S. Grouni, and M. S. Boucherit, "Improved MPPT control strategy for PV connected to grid using IncCond-PSO-MPC approach," *CSEE Journal of Power and Energy Systems*, vol. 9, no. 3, pp. 1008–1020, 2023, doi: 10.17775/CSEEJPES.2021.08810.
[26] S. Ahmadi, S. Shokoohi, and H. Bevrani, "A fuzzy logic-based droop control for simultaneous voltage and frequency regulation in an AC microgrid," *International Journal of Electrical Power & Energy Systems*, vol. 64, pp. 148–155, Jan. 2015, doi: 10.1016/j.ijepes.2014.07.024.
[27] R. Hu *et al.*, "An interleaved bidirectional coupled-inductor based DC–DC converter with high conversion ratio for energy storage system," *IEEE Transactions on Industrial Electronics*, vol. 69, no. 6, pp. 5648–5659, Jun. 2022, doi: 10.1109/TIE.2021.3091926.
[28] L. Yu, L. Wang, C. Yang, L. Zhu, Y. Gan, and H. Zhang, "A novel nonisolated GaN-Based bidirectional DC–DC converter with high voltage gain," *IEEE Transactions on Industrial Electronics*, vol. 69, no. 9, pp. 9052–9063, Sep. 2022, doi: 10.1109/TIE.2021.3113015.

BIOGRAPHIES OF AUTHORS

Sebin Davis Kurichiparambil was born in Thrissur, (KL) India. He obtained his B.Tech. in Electrical and Electronics Engineering from Cochin University of Science and Technology (KL) and M.Tech. in Power Electronics from Calicut University (KL), India, in 2009 and 2012, respectively. Presently, he is working is Sahrdaya Engineering College, Thrissur, and pursuing his Ph.D. in EED at Karunya Institute of Technology and Sciences, Coimbatore, India. His area of interest includes power electronics and renewable energy integration to the grid. He can be contacted at email: sebindavisk@gmail.com.

Dr. Varghese Jegathesan is received the B.E. and M.E. degrees from Bharathiar University, Coimbatore, India, in 1999 and 2002 respectively and the Ph.D. degree from Anna University, Chennai, India, in 2010. Currently, he is an associate professor in the Department of Electrical and Electronics Engineering at Karunya Institute of Technology and Sciences, India. He has presented technical papers at various national and international conferences in India and Abroad. He has also published papers in national and international peer-reviewed journals. His area of interest includes electric circuits and networks, power electronics, the development of heuristic algorithms for power electronics applications and the application of power electronics to renewable energy. He can be contacted at email: jegathesan@karunya.edu.